ACS Catalysis

pubs.acs.org/acscatalysis

Research Article

Catalyst Deactivation Processes during 1-Hexene Polymerization

Anuj Joshi, Harmen S. Zijlstra, Scott Collins, and J. Scott McIndoe*

Cite This: *ACS Catal.* 2020, 10, 7195−7206

Read Online

ACCESS | Metrics & More | Article Recommendations | Supporting Information

ABSTRACT: The catalyst $[Cp_2Zr(\mu\text{-}Me)_2AlMe_2]^+[B(C_6F_5)_4]^-$ (**1**) has been studied by electrospray ionization mass spectrometry in order to better understand the complexities of catalyst deactivation in the polymerization of 1-hexene. Using off-line, online, and flow-based methods, we observe that zirconium π-allyl species are unstable in solution and previously unobserved dimethylalane complexes are more stable. The dimethylalane complexes are resistant to further 1-hexene additions, and their formation represents a previously unrecognized pathway for catalyst deactivation.

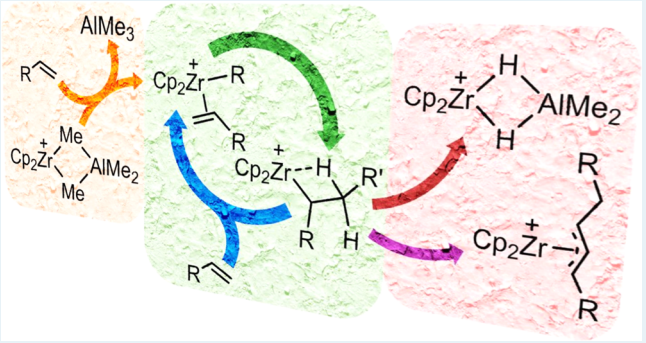

KEYWORDS: *olefin polymerization, metallocene catalyst, electrospray ionization, mass spectrometry*

INTRODUCTION

In situ monitoring of olefin polymerization,[1] mediated by metallocene or other transition-metal catalysts, has emerged as a powerful tool for detection of initiators, resting states, and deactivation reactions inherent to these complex catalyst systems.[2] A variety of spectroscopic techniques, including UV−vis[3] and NMR spectroscopy,[4] have been applied to this problem. Impressive gains in sensitivity have been achieved using NMR and an isotopically labeled[5] or hyperpolarized monomer,[6] combined with specialized flow or stopped-flow reactors.[7] NMR spectroscopy remains the definitive method for structural characterization of reactive intermediates,[8] though model compounds are often employed to confirm in situ spectroscopic assignments.[9] Mass spectrometric methods have also been employed to study a variety of catalytic processes[10,11] including olefin polymerization[12] with electrospray ionization mass spectrometry (ESI-MS) emerging as a sensitive and potent method for both detecting and identifying catalyst intermediates in solution[13−15] and for studying their reactivity in the gas phase.[16]

These studies have revealed a wealth of information—the nature of the catalyst resting states is dependent on catalyst structure, the method of activation, the nature of the counterion, and even the monomer.[2] In the case of discrete metallocenium ions, generated in situ from metallocene dialkyls and activators such as $B(C_6F_5)_3$ or $[Ph_3C][B(C_6F_5)_4]$, dormant states are π-allyl complexes formed in situ via C−H activation of α-olefins or unsaturated chain ends.[17] The extent to which these well-studied complexes are competent for further chain growth is dependent on the catalyst, counterion, and monomer.[18,19] In other cases, where the (unhindered) metallocene is prone to β-H elimination, dormant contact ion pairs such as $Cp_2ZrR(\mu\text{-}HB(C_6F_5)_3)$ are formed using borane-activated catalysts,[20] which can be rather resistant to further insertion.[21]

In methylaluminoxane (MAO)-activated metallocenes, where Me_3Al is inevitably present as a chain-transfer agent, the π-allyl species are also detected,[22] though their concentration is lower than that of the main chain-carrying $[Cp_2Zr(\mu\text{-}R)(\mu\text{-}Me)\text{-}AlMe_2]^+$ complexes identified some time ago by Brintzinger and Babushkin.[5] Further, in MAO-activated systems, the π-allyls appear susceptible to chain transfer to Al, which provides another mechanism for catalyst reactivation.

In another work featuring the use of $i\text{-}Bu_3Al$ as an alkylating agent/scavenger and $[Ph_3C][B(C_6F_5)_4]$ as an activator, π-allyl cations can form in situ.[23] However, the principal resting state during polymerization in the case of $i\text{-}Bu_2AlH$ features $[Cp_2ZrR]$ cations stabilized by coordination of $i\text{-}Bu_2AlH$ forming trinuclear Zr,Al_2 complexes with strong Zr−H−Al bridging.[24] Given the presence of $i\text{-}Bu_2AlH$ in $i\text{-}Bu_3Al$ solutions, one suspects that these intermediates may play a role in olefin polymerization in a catalyst system developed many years ago—viz. $Cp_2ZrCl_2/R_3Al/[Ph_3C][B(C_6F_5)_4]$,[25] as an alternative to MAO-activated catalysts.[26]

Hexene has often been employed as a model monomer in these studies as a surrogate for more reactive monomers such as propene or ethylene. The latter are difficult to study, depending on the activator, as mass-transfer effects can dominate,[27] while

Received: April 8, 2020
Revised: June 2, 2020
Published: June 3, 2020

the tactic or crystalline polymers formed are generally insoluble and can complicate the kinetics.[28] Further, at least one study has established that the rates of hexene polymerization are insensitive to the nature of the counterion, while propene shows much wider variations.[29]

Under typical conditions in hydrocarbon media, the recent work of Kissin where gas chromatography−MS was used to study the hexene oligomer distribution in the case of Cp_2ZrCl_2 and MAO activation is instructive.[30] There was a line of evidence for chain transfer to Me_3Al, β-H elimination, and a minor secondary insertion under the conditions studied (neat hexene, 50−100 °C, hydrolytic vs nonhydrolytic MAO). It should be noted that an incomplete monomer conversion was observed (50−75% conversion at or below 80 °C), and though not commented upon, that behavior is consistent with catalyst deactivation.

Hilty and co-workers also studied hexene polymerization using $[Cp_2ZrMe]^+$ in ca. 90:10 toluene/PhF mixtures with [Zr] = 2−19 mM and [hexene] = 0.283 M at room temperature.[6] Using special injection and mixing techniques, involving a hyperpolarized monomer, they were able to acquire ^{13}C spectra within 0.45 s of mixing and estimated k_p = 95 M^{-1} s^{-1} for consumption of monomer over a 12 s period. They invoked rapid decay of the propagating species under these conditions (from the biexponential decay curves seen for hexene consumption) and concluded that this deactivation process led to π-allyl formation with $k_d \approx 0.88$ s^{-1}. Hexene consumption is about 30× faster than catalyst deactivation at a constant monomer concentration.

Norton and co-workers studied carboalumination of allylbenzene at 40 °C using $[(EBI)Zr(\mu\text{-}Me)_2AlMe_2][B(C_6F_5)_4]$ (EBI = *rac*-1,2-ethylenebis(η^5-indenyl)) with [Zr] = 0.38 mM, [allylbenzene] = 2.55 mM, and a large excess of Me_3Al (>50:1 Al/Zr).[31] They obtained $k_{obs} = 5.1 \times 10^{-4}$ s^{-1} at [Al] = 61 mM corresponding to a second-order rate constant of 1.3 M^{-1} s^{-1} for consumption of allylbenzene at this higher temperature. The behavior of $[Cp_2Zr(\mu\text{-}Me)_2AlMe_2][B(C_6F_5)_4]$ (**1**) was not studied in the same level of detail but appeared similar.

Finally, in a very recent study employing UV−vis spectroscopy, Brintzinger and co-workers studied hexene polymerization using $[(SBI)Zr(\mu\text{-}Me)_2AlMe_2][B(C_6F_5)_4]$ (SBI = *rac*-$Me_2Si(\eta^5\text{-indenyl})_2$) in benzene solution with k_p = 135 M^{-1} s^{-1} and [Zr] = 0.5 mM.[19] They concluded that the propagating species formed two kinds of π-allyl complexes. Those formed from direct C−H activation of terminal alkenes (including hexene) were unreactive toward further monomer insertion, while those formed from iso-alkenes, formed following β-H elimination, were sluggishly reactive. The latter type also underwent slow reactivation through chain transfer to excess Me_3Al.

Over the past several years, we have applied ESI-MS to the study of MAO activation of metallocene complexes in fluorobenzene (PhF) solution, where both cationic and anionic species can be readily detected and characterized.[32,33] We have also studied ion speciation in the case of additives such as octamethyltrisiloxane (OMTS), which forms a well-defined ion pair $[Me_2Al(OMTS)][(MeAlO)_{16}(Me_3Al)_6Me]$ through the process of $[Me_2Al]^+$ abstraction from MAO.[34] This additive has proven useful in monitoring both aging and oxidation of MAO,[35,36] features known to be important in affecting the efficacy of this elusive but important activator.[37−39]

We have also studied the reaction of MAO-activated Cp_2ZrMe_2 with ethylene in toluene solution at low ethylene pressures.[40] In that case, a hitherto undetected, but long-suspected process for catalyst deactivation[41] was revealed by ESI-MS—formation of inactive, dinuclear Zr_2 complexes arising from the reaction of active species (i.e., $[Cp_2ZrR]^+$) with each other, as shown through experiments with labeled ethylene-d_4.

During that study, we briefly explored the use of in situ reaction monitoring via pressurized sample infusion (PSI)[42] to study ethylene polymerization in PhF solution using a diluted monomer (99:1 ethane/ethylene mixture) as both the reactant and pressure source. Considerable difficulty was encountered in pumping dilute MAO solutions via the PSI technique because of incipient clogging issues (i.e., formation of boehmite gel at the spray tip or along the flow path, which included an in-line filter to remove the solid polyethylene). These features gave rise to both random and systematic variations in flow rate as well as spray instability arising from the latter. This has a negative effect on the appearance of the total ion chronogram, which renders collection of reliable kinetic data problematic. We thus decided to focus on 1-hexene polymerization using the MAO-free catalyst system $Cp_2ZrMe_2/Me_3Al/[Ph_3C][B(C_6F_5)_4]$.

Because ESI-MS (and PSI) requires the use of a polar solvent, these studies have been conducted mainly in PhF solution. We have shown a strong analogy between these conditions when it comes to catalyst activation using MAO versus other spectroscopic studies in toluene solution.[33] In this more polar solvent, ion pairing and aggregation phenomena, involving outer-sphere ion pairs, are bound to be less pronounced than in hydrocarbon media.[43] One expects an increase in catalytic activity, at least with strongly ion-paired systems.[44,45] However, it has been shown that catalyst stability can be higher in the aggregated phase in benzene solvent.[46]

The results in this paper are organized into sections. First, we study in situ catalyst activation to determine optimal conditions for catalyst formation. Under these optimal conditions, we then study monomer consumption and the oligomeric products formed using ^1H NMR spectroscopy. We then examine catalyst speciation under a constant monomer concentration in a continuous process and both off-line and PSI studies under batch conditions to study both short- and long-term catalyst speciation. We anticipate that the results are highly relevant to batch hexene polymerizations in hydrocarbon media using this catalyst and activator, at least at lower temperatures.

RESULTS—CATALYST ACTIVATION

The synthesis of $[Cp_2Zr(\mu\text{-}Me)_2AlMe_2][B(C_6F_5)_4]$ (**1**) has been described and involves addition of excess Me_3Al to $[Cp_2ZrMe][B(C_6F_5)_4]$ (**2**) generated in situ from Cp_2ZrMe_2 and $[Ph_3C][B(C_6F_5)_4]$ at a low temperature.[47] High isolated yields are obtained upon subsequent crystallization. However, we wondered whether we could monitor this activation process at room temperature in PhF solvent using ESI-MS. Besides the use of PhF, this approach mimics what is typically done in olefin polymerization studies—that is, in situ catalyst generation.

One basic approach involved simultaneous pumping of a solution of $[Ph_3C][B(C_6F_5)_4]$ in PhF solution and a separate solution of Cp_2ZrMe_2 and Me_3Al in PhF into a mixing tee inside a glovebox with a short length of polytetrafluoroethylene tubing running from the tee to the source compartment of the mass spectrometer.[15] By varying the flow rate through the mixing tee, one obtains "snapshots" of the instantaneous product distribution at various time scales in a continuous process.

An example of the data obtained is shown in Figure 1. At a 2:1 Al/Zr stoichiometry, formation of $[Cp_2Zr(\mu\text{-}Me)_2AlMe_2]^+$ (**1**

https://dx.doi.org/10.1021/acscatal.0c01607
ACS Catal. 2020, 10, 7195−7206

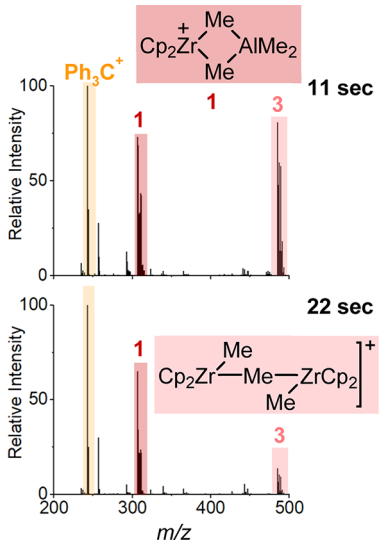

Figure 1. Monitoring of catalyst activation using $[Ph_3C][B(C_6F_5)_4]$ (0.31 mM), Cp_2ZrMe_2 (0.31 mM), and Me_3Al (0.61 mM). Representative mass spectra after 11 and 22 s are shown.

m/z 307) and the dinuclear complex $[(Cp_2ZrMe)_2(\mu\text{-Me})]^+$ (**3** *m/z* 485) occurs at competitive rates. At longer reaction times (i.e., slower mixing rates), formation of **3** is suppressed as Cp_2ZrMe_2 is consumed and **2** is competitively trapped by Me_3Al forming **1**.

Based on these results, slow addition of a 1:2 to 1:10 mixture of $Cp_2ZrMe_2/AlMe_3$ to a rapidly stirred solution of $[Ph_3C][B(C_6F_5)_4]$ in PhF solution (basically titration to a colorless endpoint) gave the cleanest formation of $[Cp_2Zr(\mu\text{-}Me)_2AlMe_2][B(C_6F_5)_4]$ (**1**). Though these conditions were used throughout this work, we should note that catalyst activation in PhF solution involved minor anion degradation[48] as revealed by ^{19}F NMR spectroscopy (Supporting Information, Figure S24). Note that this was only observed during catalyst activation, not following addition of monomer.

Hexene polymerization experiments were conducted with solutions dominated by **1**, but **3** also reacted with hexene, confirming that both **1**[47] and **3**[49] act as reservoirs of **2**. We attempted to generate **2** in situ by the addition of Cp_2ZrMe_2 to 1 equiv of $[Ph_3C][B(C_6F_5)_4]$ in PhF solution. At [Zr] = 4.0 mM, the reaction affords a mixture of **2** and **3**. The direct reaction between Cp_2ZrMe_2 and $[Ph_3C][B(C_6F_5)_4]$ is slower in comparison to reactions conducted in the presence of Me_3Al. It is known that competing formation of **3** impedes activation of Cp_2ZrMe_2.[47,49]

Trace amounts of a fluorobenzene complex of **2** with *m/z* 331[14,50] were also detected in this experiment (see Supporting Information Figure S1). Because the reaction was not clean, and it appears that **2** is also unstable in PhF solution, decomposing to form $[(Cp_2ZrMe)_2(\mu\text{-F})]^+$ (among other species) over a 3 h period, we focused much of our subsequent efforts on the reactivity of **1**.

Hexene Polymerization—Monomer Consumption. We monitored 1-hexene polymerization in PhF solution with [Zr] = 0.25 mM and Al/Zr = 1000:1 at room temperature with [hexene] = 0.25 M by ^1H NMR spectroscopy. A vortex mixer was used to mix the catalyst with the monomer, where the tube was cooled to −23 °C prior to addition of catalyst. A 30 s delay, corresponding to sample insertion, and locking was required before the first ^1H spectrum could be acquired with the probe at room temperature.

In agreement with the results of Hilty,[6] we observed catalyst deactivation evidenced by 25−30% conversion of monomer upon mixing. At higher [Zr] = 1.0 mM, more extensive consumption of monomer was observed (75% conversion on mixing), and now, a slower process that resulted in additional monomer consumption was detected (data are shown in Supporting Information Figures S2 and S3). This slower process featured $k_{obs} = 4.07 \times 10^{-4}$ s^{-1} or a second-order rate constant of 0.41 M^{-1} s^{-1} (roughly 100× slower than initial monomer consumption vide infra).

At lower temperature, it was possible to monitor the faster monomer consumption step, and though deviation from first-order kinetics was observed, consistent with catalyst deactivation, the limiting value for $k'_{obs} = 3.1 \times 10^{-4}$ s^{-1} or $k_p = 12.3$ M^{-1} s^{-1} at 0 °C (Supporting Information Figures S4 and S5). Neglecting any entropic component to the free energy of activation ($\Delta G‡$ = 20 kcal mol^{-1} estimated from the Eyring equation for k'_{obs} at 0 °C), one can estimate that $k'_{obs} = 0.0078$ s^{-1} at 298 K, which corresponds to a second-order propagation rate constant of ca. 31 M^{-1} s^{-1}.

This is lower than the value (95 M^{-1} s^{-1}) determined by Hilty and co-workers for the same catalyst in 90:10 toluene/PhF.[6] On the other hand, Norton and co-workers[31] established that the rate of carboalumination featured an inverse, first-order dependence on $[Me_3Al]$ with the concentration of monomeric Me_3Al being governed by the relevant dissociation equilibrium: $Me_6Al_2 \leftrightarrow 2Me_3Al$ with K_d (298 K) = 4.15×10^{-6} M.[51] The rate law they derived can be related to the current discussion through the following equation

$$\text{rate} = -\frac{d[\text{olefin}]}{dt} = \frac{k_1 k_2[\text{Zr}][\text{olefin}]}{(k_{-1} + k_2)\left(\frac{[Me_3Al]}{K'} + 1\right)} = \frac{k_p[\text{Zr}][\text{olefin}]}{\frac{[Me_3Al]}{K'} + 1}$$

where K' is the equilibrium constant for dissociation of monomeric Me_3Al from **1**. At the lower Al concentrations used here (i.e., [Al] = 2.8 mM with monomeric $[Me_3Al]$ = 76 μM), one can estimate from their value of K' at 40 °C (4.1×10^{-4} M) that only a slight retardation on insertion rates is expected (ca. 14%). However, one can expect a significant decrease in K' with a decrease in temperature and thus more significant inhibition by excess Me_3Al at lower temperatures.

Evidently, monomer (and catalyst) consumption occurs at minimum initial rates between 0.024 and 2.4 mM s^{-1} at room temperature with [Zr] = 0.28 mM depending on monomer concentration. The slower monomer consumption stage on the other hand is characterized by much more leisurely changes in [Zr] = 0.32−32 μM s^{-1} or 0.019−1.9 mM min^{-1}, and this will be important for interpreting what follows.

Unsaturated Groups in Polyhexene. The ^1H NMR spectrum recorded in PhF solution at [Zr] = 4.0 mM following the addition of 100 equiv of hexene (corresponding to starved feed conditions vide infra) was shown with respect to formation of unsaturated structures in the polyhexene produced (see Supporting Information Figure S6).

Signals due to vinylidene ($H_2C{=}CR_2$), trisubstituted vinyl ($R_2C{=}CHR$), and vinylene ($RCH{=}CHR$) protons are seen in this spectrum in the regions 4.6−4.8, 5.1−5.3, and 5.3−5.5, respectively.[52] The ratio of these groups in the polymer is

https://dx.doi.org/10.1021/acscatal.0c01607
ACS Catal. 2020, 10, 7195−7206

0.652:0.266:0.082. Allylic protons are also present, which, after correction for the presence of unreacted hexene, integrate to 4.4 protons relative to these olefinic signals. As shown in Chart 1, a ratio of 4.1:1 is expected for the structures **A**–**C**.

Chart 1. Unsaturated Groups in Poly(hexene)

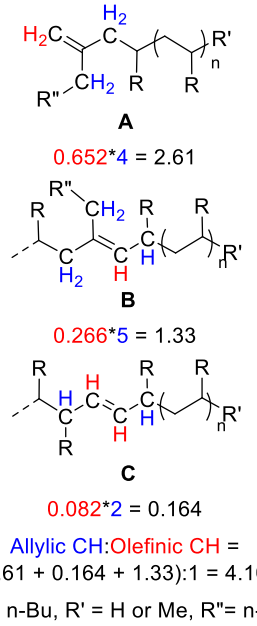

Structure **A** corresponds to the end groups formed by β-H elimination (or chain transfer to monomer) following primary 1,2-insertion of hexene into $[Cp_2ZrR]^+$ {R = Me, $-(C_6H_{12})_nH$}.[53] Structures **B** and **C** correspond to internal rather than terminal unsaturation. The accepted mechanism for forming these structures invokes C–H activation (and elimination of H_2) following β-H elimination, forming π-allyl complexes **4** or **5**, followed by further chain growth as shown in Scheme 1.[17−19]

The predominance of structure **B** over **C** reflects the preference for primary 1,2-insertion versus secondary 2,1-insertion, coupled with presumably differential reactivity of the resulting π-allyl complexes **4** and **5** toward further insertion. Evidently, under these starved feed conditions, the poly(hexene) formed presents extensive evidence for β-H elimination, coupled with C–H activation. One might expect to observe **4** and **5** during hexene polymerization based on these results.

From the ratio of the vinylidene end groups to the CH protons of the main chain, it can be deduced that the average degree of polymerization is close to 5 in this material (M_n = 420 g mol^{-1}). This corresponds to three repeat units of monomer with one saturated and unsaturated end group per chain. The intensity of the vinylidene protons with respect to the main chain (and terminal) Me groups (1:6.4 measured vs 1:5 calculated) suggests that the majority of chains initiate by insertion into Zr–H (77.5%) versus Zr–Me (22.5%). Given the 100:1 monomer/Zr ratio, roughly eight chains are produced per Zr at 38% conversion of monomer in this experiment.

Catalyst Speciation at Steady State—Constant Monomer Concentration. Solutions of activated catalyst [Zr] = 0.28 mM and a solution of monomer (1000 equiv) in PhF solution, each containing Me_3Al ([Al] = 2.8 mM), were simultaneously pumped into the mixing tee mentioned earlier. Figure 2 shows some representative mass spectra of product mixtures at

Scheme 1. Formation of Unsaturated Groups in Poly(hexene)

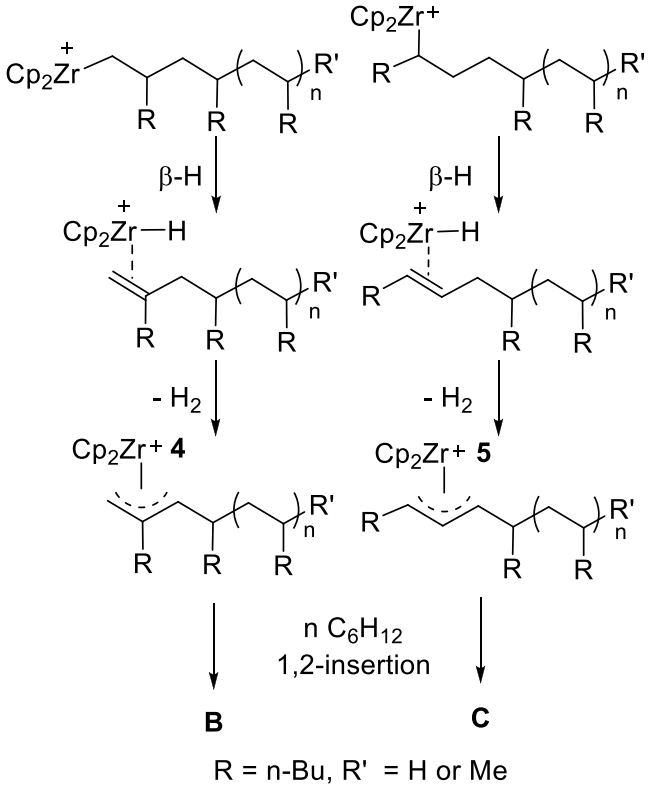

different reaction times at a 1000:1 hexene/Zr ratio. Flow rate is a proxy for reaction time, with high flow rates corresponding to a short reaction time before the mixed solution emerges into the ESI-MS source.

With lag times of 4–16 s, a mixture of ions at m/z 279, 293, 311, 363, and 471 was observed. In our earlier work,[40] ions with m/z 279, 293, and 311 were also formed in PhF solution during PSI experiments involving diluted ethylene. The ion with m/z 279 was shown to be $[Cp_2Zr(\mu\text{-H})_2AlMe_2]$ (hereinafter **6**) on the basis of its tandem mass spectrometry (MS/MS) spectrum (Supporting Information Figure S7). The ion with m/z 293 is $[Cp_2Zr(\mu\text{-H})(\mu\text{-Me})AlMe_2]^+$ (hereinafter **7**) on the basis of its MS/MS spectrum (Supporting Information Figure S8). The ion with m/z 311, like complex **7**, is more prominent in the mixture at short reaction times. Because this ion was not observed in ethylene (or hexene) polymerization experiments conducted in toluene solution,[40] it was assigned to $[Cp_2Zr(\mu\text{-F})(\mu\text{-Me})\text{-}AlMe_2]^+$ (**8**), ostensibly a product of C–F activation, a reaction that is known to be mediated by cationic zirconocene complexes in the presence of triisobutylaluminum.[54]

The MS/MS spectrum of ion **8** is not entirely consistent with this formulation; **8** readily loses 16 (CH_4) and then 66 Da (C_5H_6) at increased collision energies (Supporting Information Figure S9). It also loses 72 Da (i.e., Me_3Al) in competition with methane loss (Supporting Information Figure S10), which is analogous to the behavior observed with m/z 293 (or ion pair **1**[33]). Though this ion often dominated under starved feed conditions (see, e.g., Figure 3 at 4 min or Figure 4a,b), it could not be detected in solution using ^{19}F NMR spectroscopy.

Finally, it was observed that the intensity of this ion was maximal upon initial pumping of solutions of ion pair **1** and hexene. Prolonged pumping of these solutions led to a

https://dx.doi.org/10.1021/acscatal.0c01607
ACS Catal. 2020, 10, 7195−7206

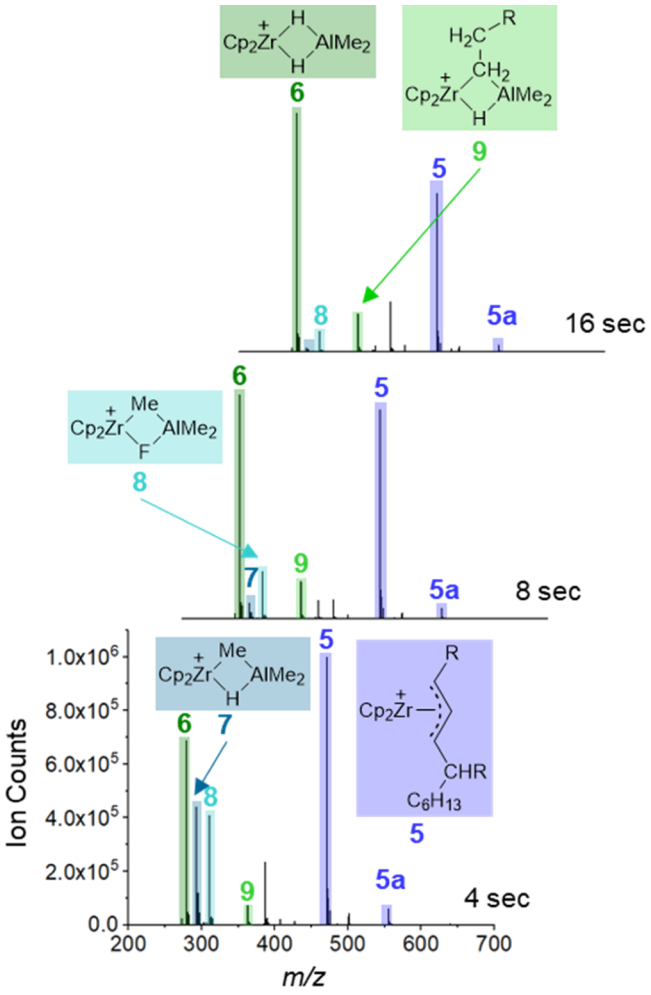

Figure 2. Positive ion ESI-MS of the product ions formed at different reaction times with hexene/Cp_2ZrMe_2 = 1000:1 in PhF solution ([Zr] = 0.31 mM); R = *n*-Bu.

pronounced decrease in the intensity of this ion relative to the others present (Figure 3). Subsequent pumping of a fresh solution of monomer and catalyst also exhibited low levels of **8**, suggesting that this ion is formed from a contaminant in the source compartment (rather than in solution), which is gradually depleted when pumping catalyst and monomer solutions.

Though we are uncertain of its structure, it is evident that it likely forms in the gas phase and involves the reaction of an impurity present with reactive Zr species that we do not detect in these experiments as there was no concomitant increase in any of the other product ions. We will discuss these issues after presenting all the data obtained.

The ion with m/z 363 fragments with an initial loss of 84 Da (i.e., hexene) to form m/z 279, followed by a 58 Da loss (Me_2AlH) to form m/z 221 $[Cp_2ZrH]^+$ (Supporting Information, Figure S11). It can thus be formulated as $[Cp_2ZrH_2AlMe_2(hexene)]^+$ (**9**), though it could also correspond to the insertion product $[Cp_2Zr(\mu\text{-}H)(\mu\text{-}n\text{-}C_6H_{13})\text{-}AlMe_2]^+$.

The relative intensities of dimethylalane adducts **6** and **9** were highly variable in this work, and experiments at different cone voltages showed that the loss of hexene from **9** occurs at low collision energies, during transit of ions from the source compartment to the high-vacuum region of the spectrometer.

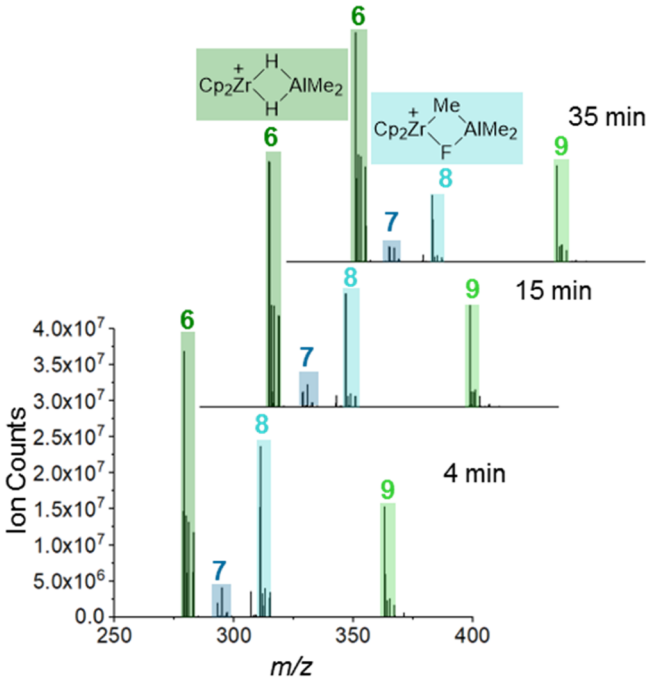

Figure 3. Mass spectra at various times following mixing of $[Cp_2ZrMe_2AlMe_2][B(C_6F_5)_4]$ (**1** [Zr] = 0.31 mM) and monomer with hexene/Zr = 10:1 in PhF solution.

Even subtle changes in pressure (and presumably atmospheric composition[55]) within the source compartment had noticeable effects on the ratio of these two ions. Similar effects have been noted before in the case of ion $[Cp_2Zr(\mu\text{-}Me)_2AlMe_2]$ (**1**), which generates ion $[Cp_2ZrMe]^+$ (**2**) via CID within the source compartment of the mass spectrometer.[33,55] Indeed, in those experiments where ion dimethylalane complex **6** was prominent, the same was true of ion **2**—prior to the introduction of hexene.

When a solution containing **9** was treated with excess *i*-Bu_3Al, substitution of the two Me groups for *i*Bu was observed (substitution of Me by *i*Bu leads to a mass difference of 42 Da), leading to formation of ions with m/z 405 and 447 (see Supporting Information Figure S17). However, no ions corresponding to substitution of a Zr- or Al-hexyl group were observed. This also supports the formulation of ion **9**, as indicated above. Note that we cannot exclude the possibility that **6** and **9** are actually in equilibrium with each other through the process of reversible binding of hexene, possibly coupled with reversible insertion (Scheme 2).

The ion with m/z 471 was quite resistant to fragmentation by MS/MS. It successively loses 2 Da (i.e., H_2) over the range in collision energies investigated (2−100 V), forming m/z 469 and at higher energy m/z 467 (Supporting Information Figures S15 and S16). Its nominal mass is consistent with the formula $[Cp_2Zr(C_6H_{10})(C_6H_{12})_2H]^+$, and the fact that it is resistant to the CID of neutral species is consistent with it being assigned as a π-allyl complex with the formula $[Cp_2Zr(\eta^3\text{-}C_6H_{10})\text{-}(C_6H_{12})_2H]^+$ (**5**). A related species with m/z 555 was also observed, which, given its mass of 84 Da above that of π-allyl complex **5**, can be assigned as the allyl complex $[Cp_2Zr(\eta^3\text{-}C_6H_{10})(C_6H_{12})_3H]^+$ (**5a**).

Catalyst Speciation during Slow Monomer Consumption. To study basic kinetics in more detail, the study of batch reactions using either off-line or PSI techniques is required.[42,56,57] The advantages of the former are convenience

https://dx.doi.org/10.1021/acscatal.0c01607
ACS Catal. 2020, 10, 7195−7206

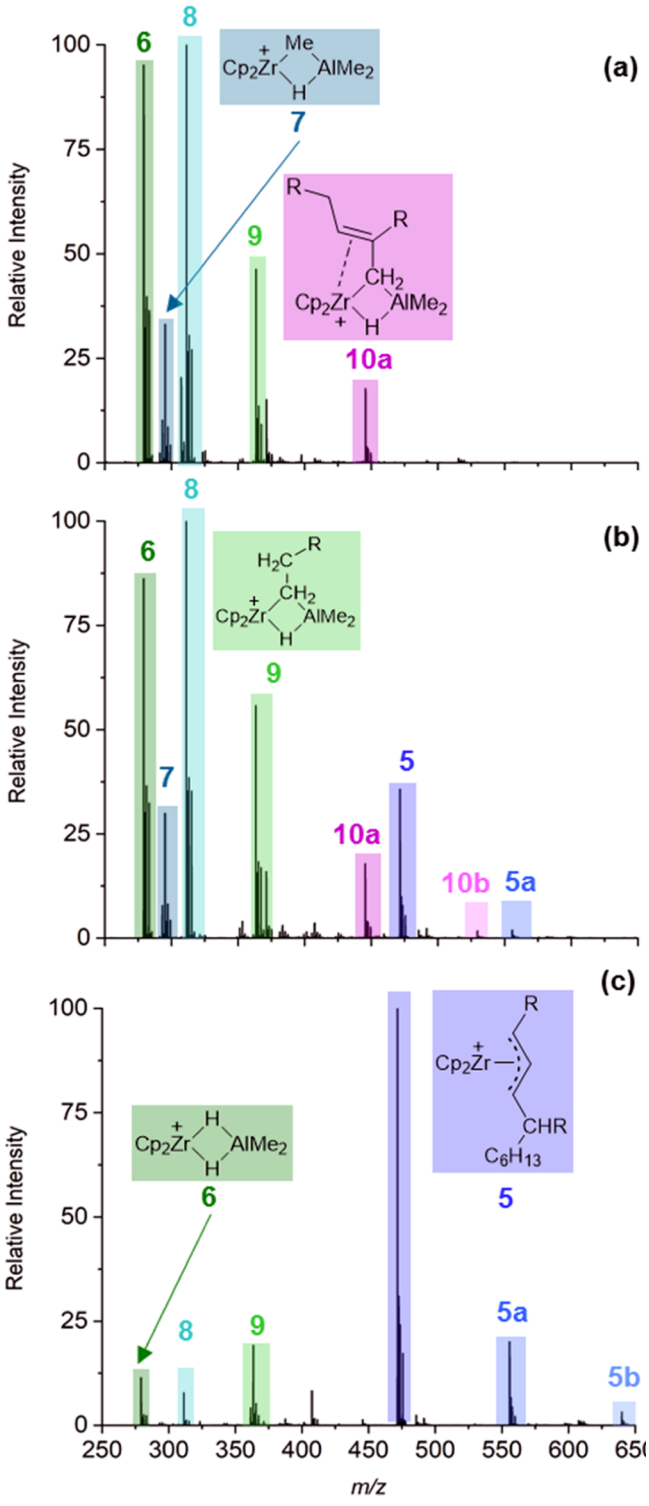

Figure 4. ESI-MS of reaction mixtures formed from 0.28 mM $[Cp_2ZrMe_2AlMe_2][B(C_6F_5)_4]$ and Me_3Al/Zr = 10:1 with (a) 10, (b) 100, and (c) 1000 equiv of hexene in PhF solution. Ions that are separated in mass by 84 Da (C_6H_{12}) are highlighted with different hues of the same color; R = *n*-Bu.

and a consistent flow rate (using a syringe pump), while PSI experiments are problematic with respect to flow rate variations in reactions of this type (because of increasing viscosity of the medium and/or incipient clogging issues, leading to variations in spray quality). On the other hand, PSI experiments feature lag

Scheme 2. Possible Equilibria between Ions 6 and 9; R = *n*-Bu.

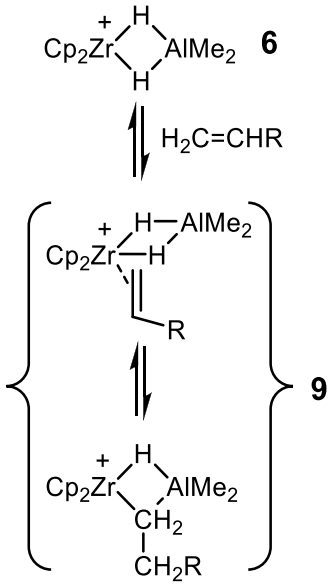

times that are comparable to those just discussed and allow direct sampling from a reaction vessel.

Off-Line Experiments—10:1 Hexene/Zr. Depicted in Figure 4 are representative mass spectra of initial mixtures obtained by adding 10−1000 equiv of hexene to the activated catalyst at [Zr] = 0.28 mM with Me_3Al/Zr = 10:1. As illustrated in Figure 4a, the mixture with 10 equiv of hexene contains ions **6**−**9**.

Also, an ion with *m*/*z* 445 (henceforth **10a**) was observed, which was much more prominent in off-line experiments compared to the flow experiments discussed previously, where it was not detected. Its MS/MS spectrum showed a low energy loss of 58 Da, followed by consecutive losses of 2 Da at higher collision energies (Supporting Information Figures S12−S14). Both lower (*m*/*z* 361, **10**) and higher homologues at *m*/*z* 529 (**10b**) and *m*/*z* 613 (**10c**), respectively, were also seen in these experiments, though with significantly diminished intensity. Collectively, formation of these products was most noticeable at low monomer/catalyst ratios. Tentatively, these related ions are assigned σ-allyl dimethylalane adducts with the formula $[Cp_2Zr\{\sigma\text{-}C_6H_{10}(C_6H_{12})_nH\}(\mu\text{-}HAlMe_2)]^+$ (**10**, *n* = 0; **10a**, *n* = 1; **10b**, *n* = 2; and **10c**, *n* = 3) and will be discussed in greater detail later.

Off-Line Experiments—1000:1 Hexene/Zr. In experiments featuring a large excess of hexene (i.e., conditions corresponding to polymerization), off-line experiments show predominant formation of π-allyl complex **5** and higher homologues separated in mass by 84 Da—that is, **5a**, **5b**, and so on (see Figure 4c). The other ions discussed above are also present but in significantly lower amounts (Figure 4c), as might be anticipated from the flow experiment presented earlier.

Though higher homologues of complex **5** were readily detected, lower-molecular-weight (MW) species (i.e., *m*/*z* 387 and 303) were present in essential trace amounts in these experiments, suggesting that formation of π-allyl complex **5** is kinetically favored. In addition to this series of ions, ions differing in mass by +14 Da were seen with weaker and variable intensity (see Supporting Information Figure S20). These are assigned as analogous π-allyl complexes but involving chains that

https://dx.doi.org/10.1021/acscatal.0c01607
ACS Catal. 2020, 10, 7195−7206

initiate with Zr−Me versus Zr−H; they were more prominent at lower monomer/Zr ratios as would be expected.

Off-Line Experiments—Time-Dependent Behavior. While monitoring these off-line experiments as a function of time, we observed that the π-allyl complexes **5**, **5a**, **5b**, and so forth were unstable in solution, while the σ-allyl ions **10**, **10a**, **10b**, and so on; dimethylalane complex **6**; and hexene adduct **9** formed at their expense. Typical data are shown in Figure 5, where we have

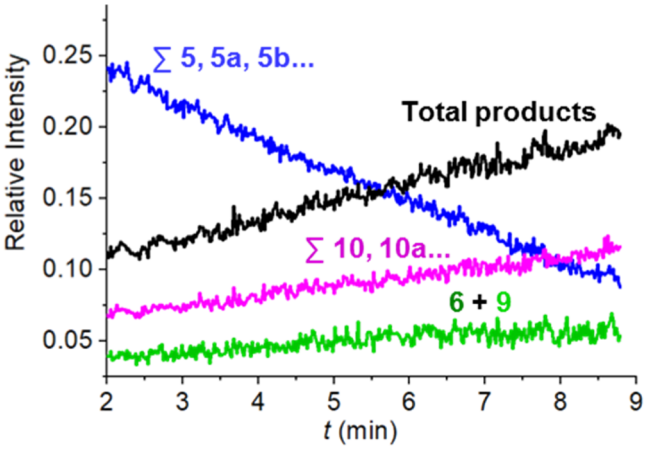

Figure 5. Sum of normalized ion intensities vs time for reaction of $[Cp_2ZrMe_2AlMe_2][B(C_6F_5)_4]$ with 1000 equiv of hexene in PhF solution.

estimated the rate of formation of **10** (m/z 361) from the normalized intensity of its first two isotope peaks and hexene adduct **9** (m/z 363) from its last four isotope peaks, corrected for the complete isotope pattern (see Supporting Information Figures S13, S14, and S18 for details).

Note that the rate of disappearance of **5**, **5a**, **5b**, and so on is linear with time in this experiment (ca. 1.5 half-lives). Assuming that the initial normalized intensity represents the fraction of catalyst **1** initially converted to these products (i.e., ca. 25%), the rate of disappearance of the π-allyls corresponds to 0.10 μM s^{-1}, which is considerably lower than slow monomer consumption discussed previously (ca. 32 μM s^{-1} at 1000 equiv of hexene).

Repetitive Monomer Addition Experiments. Though the transient behavior observed above could contribute to slow monomer consumption observed at higher [Zr], the reactivity of ions dimethylalane complex **6** and hexene adduct **9** toward the monomer has not been demonstrated, and yet these ions are formed at the earliest stages of polymerization, at least under starved feed conditions. We examined this by looking at repetitive additions of hexene to a mixture of these ions using PSI techniques.

As shown in Figure 6, addition of 20 equiv of hexene to a solution of **1** (0.25 mM) led to rapid consumption of this ion with the formation of dimethylalane complex **6** and hexene adduct **9** as the principal products. Further additions of hexene did not lead to consumption (or further growth) of these products, even transiently. During these additions, slow growth of σ-allyl **10a** is observed, but as it is nearly continuous and unperturbed by the further additions of monomer, it is not obvious that either **6** or **9** are the precursors to this material. The fact that monomer insertion is involved is evident from the higher MW of **10a** relative to either possible precursor.

It may be a very unfavorable, pre-equilibrium for dissociation of Me_2AlH from either **6** or **9** that is rate-determining in forming

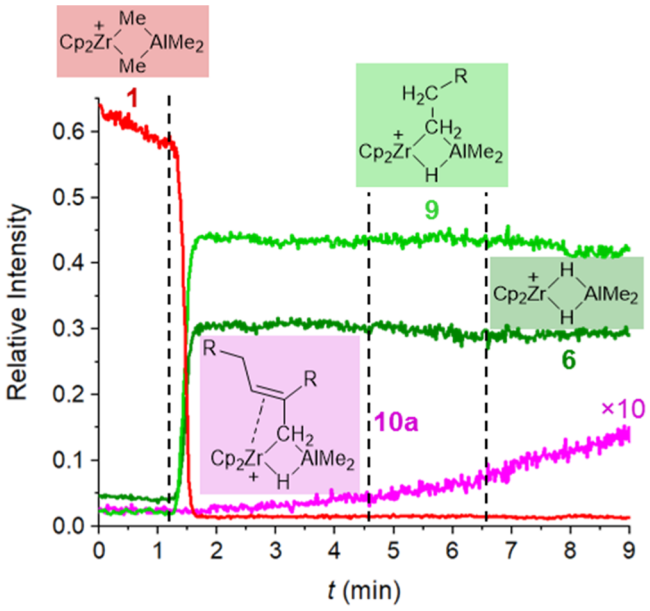

Figure 6. Normalized ion intensities vs time for sequential additions of 20 equiv of hexene to $[Cp_2ZrMe_2AlMe_2][B(C_6F_5)_4]$ (0.25 mM in PhF solution). Vertical dashed lines indicate the additions of hexene, while the intensity of the ion **10a** has been expanded 10-fold; R = *n*-Bu.

10a. A similar behavior is exhibited by $[L_2HfH_2Al^iBu_2][B(C_6F_5)_4]$ formed in situ from L_2HfCl_2, excess TiBAl, and $[Ph_3C][B(C_6F_5)_4]$ (L_2 = 1,2-C_2H_4(Flu)(5,6-C_3H_6-2-MeInd) on addition of propene.[58]

This experiment shows that formation of dimethylalane complex **6** and hexene adduct **9** is accompanied by catalyst deactivation or, to be fair, much slower monomer consumption compared to initial rates. Though we hesitate to analyze the buildup of **10a** in this experiment, given the variable monomer concentrations, the pseudo-first-order rate constant for this ($k_{obs} \leq 1.4 \times 10^{-4}$ s^{-1}) is the same order of magnitude as that determined for slow monomer consumption (vide supra).

PSI Experiments. The initial work of this type focused on the use of PhF as a solvent. However, we experienced considerable difficulty using this solvent and this technique, at least within the confines of a glovebox and using a simple apparatus such as that described in the literature.[42] However, better results were obtained using the more polar solvent *o*-difluorobenzene (ε = 13.4, *o*-$C_6H_4F_2$),[59] which is of similar volatility as PhF. Fortunately, the product distributions just discussed in detail were less perturbed by this solvent choice, while considerably more intense spectra were seen using this solvent. In Figure 7 are shown two experiments of this type at [Zr] = 0.28 mM with addition of 10 or 1000 equiv of monomer, with major ions illustrated.

Note that in Figure 7a, consumption of ion **1** is incomplete. This is expected as dissociation of Me_3Al from this ion is less favorable than for higher analogues,[31] while ion pairing in the resulting 14e species is expected to be tighter as well, leading to the well-known phenomenon that the first insertion of monomer (with rate constant k_i) is generally quite a bit slower than the subsequent insertions.[17,53]

In fact, from Figure 7a, where conversion of ion **1** is ca. 80% and using the equation $n = -(k_p/k_i)\ln([Zr]/[Zr]_o) - (1 - (k_p/k_i))[([Zr]/[Zr]_o) - 1]$, where n = amount of equiv of monomer added,[60] we can estimate that $k_p/k_i = 11$. Also, the limiting slope for this curve at t = 0 corresponds to an initial insertion rate

https://dx.doi.org/10.1021/acscatal.0c01607
ACS Catal. 2020, 10, 7195−7206

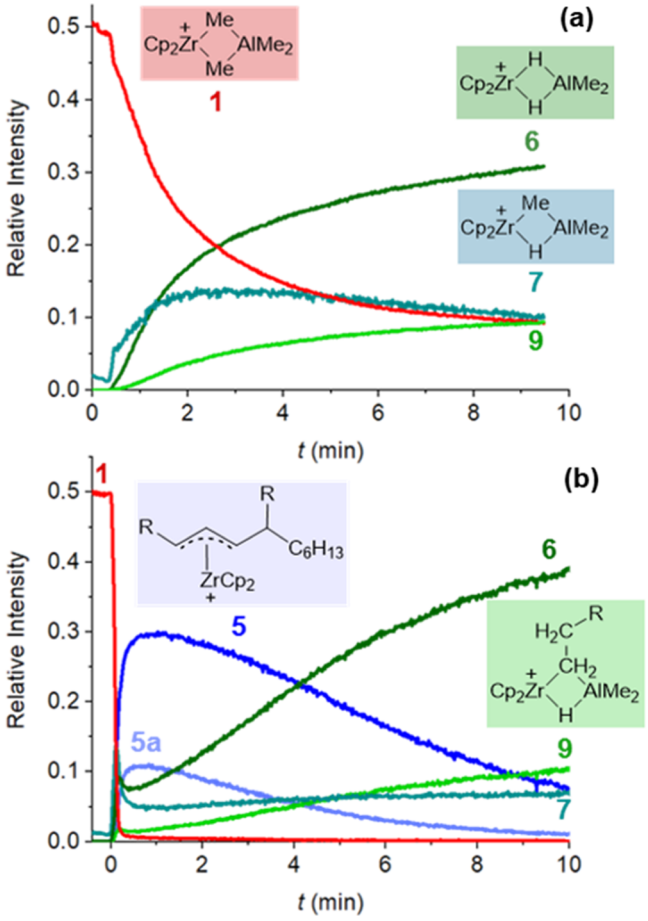

Figure 7. Normalized ion intensities vs time for addition of (a) 10 and (b) 1000 equiv of hexene to $[Cp_2ZrMe_2AlMe_2][B(C_6F_5)_4]$ in PhF_2 solution with [Zr] = 0.28 mM; R = *n*-Bu.

constant of k_i = 3.3 M^{-1} s^{-1}. This gives an estimate of k_p = 36 M^{-1} s^{-1}, which is in reasonable agreement with that estimated from extrapolation from NMR data at 0 °C for rapid monomer consumption.

Note the initial appearance of ion **7** in Figure 7a. Both this ion and ion **8** appear at the earliest times in these PSI experiments, consistent with them forming most rapidly from the starting material (see also Figure 2). Under starved feed conditions, evidently, **7** is the primary product formed, while formation of ions dimethylalane complex **6** and hexene adduct **9** involve additional steps. In particular, complex **7** might form directly from $[Cp_2Zr(\mu\text{-R})(\mu\text{-Me})AlMe_2]$ via β-H elimination, supposing that the propagating ions in this case are the same as those identified by NMR quite some time ago by Babushkin and Brintzinger.[5]

The second experiment at a 1000:1 monomer-to-catalyst ratio exhibits a plethora of transient behavior at both short and long time length scales, fully consistent with all prior experiments. Basically, the rapid formation of **7** (and **8**), subsequent formation of dimethylalane complex **6** and hexene adduct **9**, concomitant formation, and subsequent disappearance of π-allyl complex **5** and homologues (**5a**, **5b**, etc.) are beautifully illustrated in this experiment.

It is very clear from these two experiments that the π-allyl complexes **5** only form in the presence of a large excess of hexene and at a time scale that is similar to the formation of **6** and **9** under these conditions. They clearly transform under longer time scales to **6** and **9** in this experiment, where we have shown that these two ions are much less reactive toward the monomer.

The kinetic behavior observed in this experiment is strongly reminiscent of that recently reported by Brintzinger and coworkers under similar conditions;[19] rapid consumption of the starting ion pair with π-allyl intermediates was detected at both short and long time scales by UV−vis spectroscopy. Though we have not monitored these reactions by UV−vis spectroscopy, there is an obvious color change (to pale orange yellow) upon adding the monomer to $[Cp_2ZrMe_2AlMe_2][B(C_6F_5)_4]$ (which is basically colorless), and though this color persists during the PSI experiment, the final solutions (which contain very little π-allyl complex **5**) are colorless.

Their basic conclusion was that π-allyl complexes form at both of these time scales with some competent for further insertion versus relatively unreactive. In their work, they also observed species at short time scales, which they assigned to the 14e propagating alkyls $[(SBI)ZrR]^+$, though their presence was deduced from deconvolution of the observed spectra, rather than direct observation.

In our case, we do not detect these species via ESI-MS, and we believe that in the case of hexene, they are just too prone to β-H elimination (forming dimethylalane complex **7**) or reactive toward impurities (forming **8**) in the source compartment. However, we suspect that the time dependence of these ions does closely track with the propagating ions, and this accounts for the PSI or other results obtained at short reaction times (Figure 2, see also Supporting Information Figures S15, S16, and S21−S22).

Finally, as shown in Figure 8, under starved feed conditions (i.e., 10 equiv of monomer), the formation of σ-allyl ions **10a**,

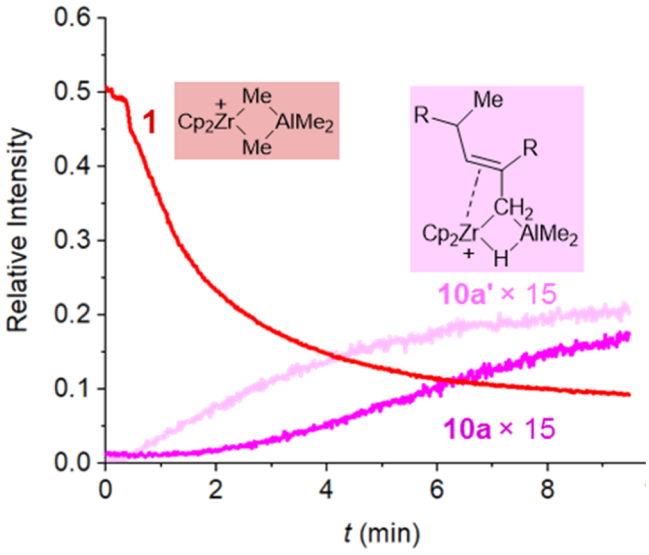

Figure 8. Normalized ion intensities vs time for addition of 10 equiv of hexene to $[Cp_2ZrMe_2AlMe_2][B(C_6F_5)_4]$ in PhF_2 solution with [Zr] = 0.28 mM. The intensities of ions **10a** and **10a**′ are expanded 15-fold, while **1** is not expanded; R = *n*-Bu.

10b, and so on can be detected, along with ions at *m*/*z* 375, 459, 543, and so on, with the latter more intense than the former, at least initially. The ion with *m*/*z* 361 (**10**) is not detected with significant intensity in this PSI experiment but is evident when larger amounts of monomer are added initially (Figure 5). The ion with *m*/*z* 459 (thenceforth **10a**′) forms directly during consumption of **1**, while there is a distinct lag phase in forming

https://dx.doi.org/10.1021/acscatal.0c01607
ACS Catal. 2020, 10, 7195−7206

10a. As the ion series **10'** differs from the "parent" series of **10** by +14 Da, it is probable that these ions are formed by insertion of hexene into Zr−Me versus Zr−H.

Finally, one should inquire as to whether any of these monitoring experiments are relevant to polymerization in hydrocarbon media. We have examined hexene polymerization in toluene solution using Cp_2ZrMe_2 activated by both MAO (100 equiv) and $Me_3Al/[Ph_3C][B(C_6F_5)_4]$ under conditions similar to those used in PhF solution. Unfortunately, it not possible to electrospray these solutions, while 10-fold dilution with PhF requires the use of fairly concentrated solutions initially. The quality of the resulting spectra, particularly in the case of trityl borate activation, is not high, but the same ions are produced under starved feed conditions as discussed above (Supporting Information Figure S23). In the case of MAO activation, the results are rather simple with the mixture consisting predominantly of alane adducts **9** and **10a**.

DISCUSSION

The formation of ions featuring coordinated Me_2AlH (i.e., **6**, **7**, **9**, and **10** and **10a** and homologues) in these experiments and at the earliest stages of polymerization is without precedent as far as we know. The fact that Me_2AlH would strongly bind to a **14e** metal alkyl or hydride is not surprising.[24,58] Efficient trapping of a π-allyl complex to form **10**, **10a**, and so forth seems less likely but cannot be excluded; trapping of an unobserved $[Ph_2C(Flu)(Cp)Zr(\eta^3\text{-}(H_2C)_2CMe)][B(C_6F_5)_4]$ intermediate by DiBAlH was invoked as a possible mechanism for forming $[Ph_2C(Flu)(Cp)Zr(\mu\text{-H-Al}^i\text{Bu}_2\text{CH}_2(\eta\text{-C(Me)}{=}\text{CH}_2))][B(C_6F_5)_4]$ in situ from $Ph_2C(Flu)(Cp)ZrCl_2$, excess TiBAl, and $[PhNHMe_2][B(C_6F_5)_4]$.[61]

Given that ions such as dimethylalane complexes **6** and **9** are resistant to further insertion, their predominant formation under starved feed conditions represents a hitherto unappreciated mechanism for catalyst deactivation or dormancy. In order to generate Me_2AlH in solution, a propagating intermediate would have to undergo β-H elimination, trapping of $[Cp_2ZrH]^+$ by Me_3Al to form ion **7**, which we do observe, and regeneration of $[Cp_2ZrMe]^+$ with the release of Me_2AlH, which we do not observe (Scheme 3). It is anticipated that the driving force for formation of **6** versus **7** from propagating intermediates $[Cp_2Zr(\mu\text{-R})(\mu\text{-Me})AlMe_2]$ is the stronger bridging for Al−H versus Al−R bonds.

Me_2AlH is strongly associated under all conditions in solution; the monomeric form has not even been detected in the gas phase.[62] The association of monomeric R_2AlH into higher oligomers has been studied theoretically.[63] For R = *i*-Bu, formation of, for example, a dimer from the monomer has $\Delta G = -20.8$ kcal mol^{-1} at 298 K in toluene, while the cyclic trimer is the most stable form. From this paper, and based on the calculated enthalpy change for R = Me, which is nearly identical (Me_2AlH is also trimeric in solution[62]), one can estimate that monomeric $[Me_2AlH] \sim 10^{-10}$ M under the conditions studied here.

If we consider the behavior shown in, for example, Figure 5 where formation of ions **6**, **9**, and **10** and homologues involves trapping of various 14- or 16e-species by Me_2AlH, the total rate of these processes is ca. 10^{-7} M s^{-1}. If we divide this by the average concentration of these species (ca. 0.042 mM), and the equilibrium concentration of monomeric Me_2AlH, the estimated second-order rate constant for trapping is 2.4×10^8 M^{-1} s^{-1}, assuming that the process is rate-determining. This in turn implies that any preceding steps involved in forming, for example, $[Cp_2ZrH]^+$ (or π-allyls) are faster, including β-H elimination or C−H activation.

Scheme 3. Proposed Formation of Me_2AlH and Its Complexes; pHx = Poly(hexenyl), R = *n*-Bu

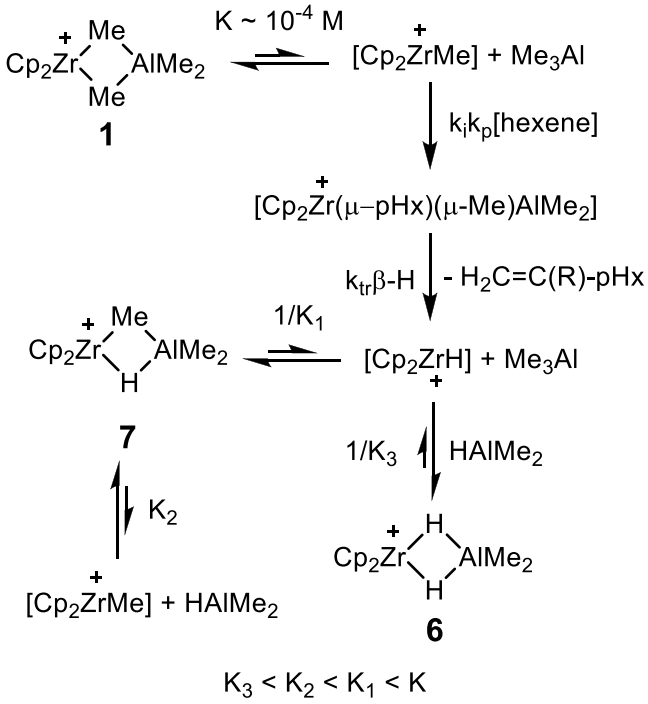

There is simply no precedent for this—the rates of these chain transfer or deactivation processes are certainly lesser than those of propagation (10^2 to 10^3 M^{-1} s^{-1}). This means trapping cannot be rate-determining; a more likely scenario is where initial insertion into **6** or **9** (leading eventually to, e.g., a π-allyl complex) is rate-limiting because of, for example, an unfavorable equilibrium for dissociation of Me_2AlH. It can be shown, subject to the steady-state approximation for any intermediates, that the rate of σ-allyl **10** formation in Figure 5 will be governed by the rate law shown below

$$\frac{d[\sigma\text{-allyl } \mathbf{10}]}{dt} = k_i K_3 \frac{[\mathbf{6}][C_6H_{12}]}{[Me_2AlH]}$$

where k_i is the rate of insertion of monomer into Zr−H, while K_3 is the equilibrium governing dissociation of Me_2AlH from **6** (Scheme 3). Of course, we do not know what K_3 is, though it is reasonable to expect that it is similar in magnitude for dissociation of $(Me_2AlH)_2$. Under this assumption, one can estimate that k_i = 290 M^{-1} s^{-1}, which is larger than that for insertion of hexene into Zr−R (31−36 M^{-1} s^{-1} here or 100−150 M^{-1} s^{-1} under other conditions). The fact that insertion into Zr−H is faster than for Zr−R seems reasonable, and the very unfavorable pre-equilibrium [$K = 5.8\ 10^{-16}$ M for $(Me_2AlH)_2$][63] accounts for the apparent lack of reactivity of ions such as **6** toward insertion of hexene.

How are we to interpret the behavior observed under more conventional conditions—as shown in Figure 7b? Evidently, ions such as **6**−**9** are transiently formed, perhaps in part due to inefficient mixing in either experiment. PSI or off-line experiments, where activated catalyst was added last to efficiently stirred monomer solutions, showed consistently lower levels of these ions (see Supporting Information Figure S19).

https://dx.doi.org/10.1021/acscatal.0c01607
ACS Catal. 2020, 10, 7195−7206

However, the main kinetic event features formation of π-allyls **5**. These then undergo a much slower reaction to ironically form Me_2AlH complexes at longer time scales. Note that this does not involve direct trapping by Me_2AlH as that should form a series of ions with m/z 529, 613, 697, and so forth. These ions are seen at long reaction times, but the dominant member of that series has m/z 445 (**10a**) and starts with m/z 361 (**10**).

Further, why is formation of π-allyl **5** predominant versus lower homologues? With reference to Scheme 1, this is not expected if these π-allyl complexes are of type **4**. It makes perfect sense however if they are of type **5**. Basically, following the primary insertion of monomer into Zr−H, it is well known that the next insertion is also highly regioregular, while 2,1-insertion into branched alkyls occurs competitively with 1,2-insertion, especially with a specific metallocene catalyst.[17,53] The resulting "dormant" state[64] might be expected to undergo competitive β-H elimination and C−H activation (with liberation of H_2), forming selectively **5** and higher homologues.

In the recent work of Brintzinger and co-workers, it has been proposed that insertion and direct C−H activation of monomer (or chains with terminal vinyl groups—which are not seen here) are competitive events.[19] We see no evidence for this, or, if it occurs, the resulting π-allyls (with m/z 303, 387, etc.) would have to be efficiently trapped by free Me_2AlH to form ions we do detect (i.e., **10** with m/z 361, 445, 529, etc.).

However, the M + 14 analogues of these ions (i.e., **10′**) do form at a faster initial rate and directly during consumption of **1** under starved feed conditions. Further, this series of ions **10′** starts with m/z 375, while those that feature insertion into Zr−H (i.e., following chain transfer) start at m/z 445 (**10a**). It is therefore likely that these σ-allyls form following β-H elimination, and specifically following primary insertion into Zr−R as shown in Scheme 4.

Tentatively, it would appear that π-allyls that feature at least one terminal CH_2 group are efficiently trapped by Me_2AlH and are thus rendered inactive, while those that do not feature the terminal CH_2 group (**5** with m/z 471, 555, 639, etc.) are not, at least relative to further insertion. Alternately, the resulting adducts might be unstable with respect to chain transfer to Al, ultimately forming alane complex **6** and the other observed products (Scheme 5).

Scheme 4. Formation of Ions with m/z 445, 529, 613, Etc., vs 375, 459, 543, Etc

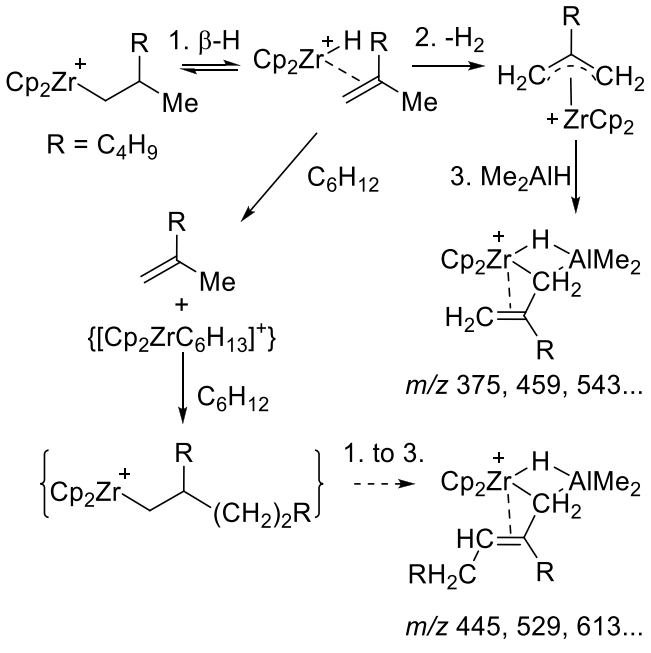

Scheme 5. Possible Reactions Consuming π-Allyl Complexes 5; pHx = Poly(hexenyl), R = *n*-Bu

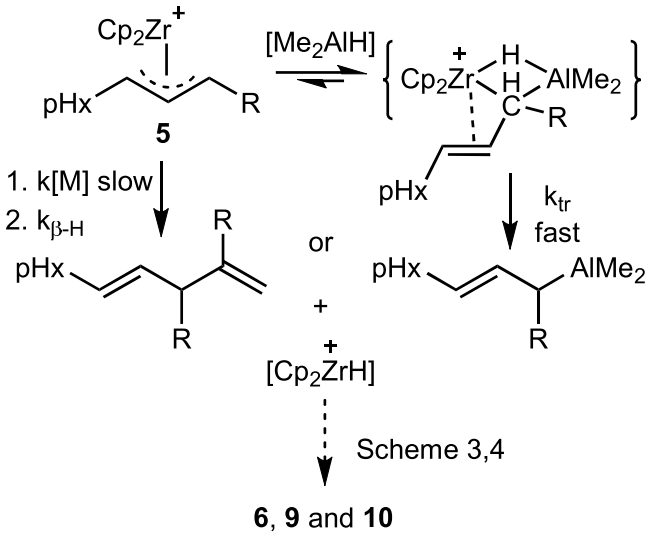

CONCLUSIONS

ESI-MS studies of hexene polymerization using $[Cp_2ZrMe_2AlMe_2][B(C_6F_5)_4]$ reveal unanticipated complexity and identification of a new pathway for catalyst deactivation—formation of dimethylalane-stabilized complexes which are resistant to further insertion. Ironically, these complexes also form under starved feed conditions, or under any condition that leads to this condition, such as poor mixing. On the other hand, π-allyl complexes dominate under other conditions, and our work suggests that they have the more hindered structure shown in Scheme 1 (type **5**) and form following 2,1-insertion. We believe that they are, in part, responsible for slow monomer consumption observed with this catalyst and that eventually all of the added catalyst pools in dormant or deactivated dimethylalane-stabilized complexes. Because the same catalysts are observed in toluene solution, we conclude that formation of dimethylalane-stabilized complexes may be a general phenomenon at least at lower temperatures.

ASSOCIATED CONTENT

Supporting Information

The Supporting Information is available free of charge at https://pubs.acs.org/doi/10.1021/acscatal.0c01607.

Experimental section, ^{1}H NMR data, MS/MS data for the ions observed, off-line data treatment, transient behavior, and modeling (PDF)

AUTHOR INFORMATION

Corresponding Author

J. Scott McIndoe − *Department of Chemistry, University of Victoria, Victoria, British Columbia V8W 2Y2, Canada;* orcid.org/0000-0001-7073-5246; Phone: +1 (250) 721-7181; Email: mcindoe@uvic.ca; Fax: +1 (250) 721-7147

https://dx.doi.org/10.1021/acscatal.0c01607
ACS Catal. 2020, 10, 7195−7206

Authors

Anuj Joshi − *Department of Chemistry, University of Victoria, Victoria, British Columbia V8W 2Y2, Canada;* orcid.org/0000-0001-7532-8607

Harmen S. Zijlstra − *Department of Chemistry, University of Victoria, Victoria, British Columbia V8W 2Y2, Canada;* orcid.org/0000-0002-5754-5998

Scott Collins − *Department of Chemistry, University of Victoria, Victoria, British Columbia V8W 2Y2, Canada;* orcid.org/0000-0001-6112-3483

Complete contact information is available at: https://pubs.acs.org/10.1021/acscatal.0c01607

Notes

The authors declare the following competing financial interest(s): Partially funded by NOVA Chemicals Centre for Applied Research.

■ ACKNOWLEDGMENTS

J.S.M. thanks NSERC (Strategic Project grant no. 478998-15) and NOVA Chemicals' Centre for Applied Research for operational funding and CFI, BCKDF, and the University of Victoria for infrastructural support. S.C. acknowledges the support for a Visiting Scientist position from the University of Victoria. The authors thank Rina Concepcion for assistance with some of the experiments, Rhonda Stoddard for conducting preliminary investigations and providing useful recommendations, and Christopher Barr for helping with NMR experiments.

■ REFERENCES

(1) Haven, J. J.; Junkers, T. Online Monitoring of Polymerizations: Current Status. *Eur. J. Org Chem.* **2017**, *2017*, 6474−6482.

(2) Bochmann, M. The Chemistry of Catalyst Activation: The Case of Group 4 Polymerization Catalysts. *Organometallics* **2010**, *29*, 4711−4740.

(3) Babushkin, D. E.; Panchenko, V. N.; Brintzinger, H.-H. Zirconium Allyl Complexes as Participants in Zirconocene-Catalyzed α-Olefin Polymerizations. *Angew. Chem., Int. Ed.* **2014**, *53*, 9645−9649.

(4) Christianson, M. D.; Landis, C. R. Generalized Treatment of NMR Spectra for Rapid Chemical Reactions. *Concepts Magn. Reson.* **2007**, *30A*, 165−183.

(5) Babushkin, D. E.; Brintzinger, H. H. Reactive Intermediates Formed During Olefin Polymerization by Methylalumoxane-Activate-dansa-Zirconocene Catalysts: Identification of a Chain-Carrying Intermediate by NMR Methods. *J. Am. Chem. Soc.* **2010**, *132*, 452−453.

(6) Chen, C.-H.; Shih, W.-C.; Hilty, C. In Situ Determination of Tacticity, Deactivation, and Kinetics in [Rac-(C2H4(1-Indenyl)2)-ZrMe][B(C6F5)4] and [Cp2ZrMe][B(C6F5)4]-Catalyzed Polymerization of 1-Hexene Using 13C Hyperpolarized NMR. *J. Am. Chem. Soc.* **2015**, *137*, 6965−6971.

(7) Christianson, M. D.; Tan, E. H. P.; Landis, C. R. Stopped-Flow NMR: Determining the Kinetics of [Rac-(C2H4(1-Indenyl)2)ZrMe]-[MeB(C6F5)3]-Catalyzed Polymerization of 1-Hexene by Direct Observation. *J. Am. Chem. Soc.* **2010**, *132*, 11461−11463.

(8) Landis, C. R.; Christianson, M. D. Metallocene-Catalyzed Alkene Polymerization and the Observation of Zr-Allyls. *Proc. Natl. Acad. Sci. U.S.A.* **2006**, *103*, 15349−15354.

(9) Vatamanu, M.; Stojcevic, G.; Baird, M. C. Detection of an η1-Alkene Intermediate of the Type [Cp2Zr(Me)(η1-alkene)]+: The Role of Such Species in Metallocene Catalyst Deactivation to Allylic Species. *J. Am. Chem. Soc.* **2008**, *130*, 454−456.

(10) Eelman, M. D.; Blacquiere, J. M.; Moriarty, M. M.; Fogg, D. E. Shining New Light on an Old Problem: Retooling MALDI Mass Spectrometry for Organotransition-Metal Catalysis. *Angew. Chem., Int. Ed.* **2008**, *47*, 303−306.

(11) Bailey, G. A.; Fogg, D. E. Confronting Neutrality: Maximizing Success in the Analysis of Transition-Metal Catalysts by MALDI Mass Spectrometry. *ACS Catal.* **2016**, *6*, 4962−4971.

(12) Gies, A. P.; Kuhlman, R. L.; Zuccaccia, C.; Macchioni, A.; Keaton, R. J. Mass Spectrometric Mechanistic Investigation of Ligand Modification in Hafnocene-Catalyzed Olefin Polymerization. *Organometallics* **2017**, *36*, 3443−3455.

(13) Vatamanu, M. Observation of Zirconium Allyl Species Formed during Zirconocene-Catalyzed Propene Polymerization and Mechanistic Insights. *J. Catal.* **2015**, *323*, 112−120.

(14) Jiang, J.; Zhang, H.; Li, M.; Dulay, M. T.; Ingram, A. J.; Li, N.; You, H.; Zare, R. N. Droplet Spray Ionization from a Glass Microscope Slide: Real-Time Monitoring of Ethylene Polymerization. *Anal. Chem.* **2015**, *87*, 8057−8062.

(15) Santos, L. S.; Metzger, J. O. Study of Homogeneously Catalyzed Ziegler-Natta Polymerization of Ethene by ESI-MS. *Angew. Chem., Int. Ed.* **2006**, *45*, 977−981.

(16) Feichtinger, D.; Plattner, D. A.; Chen, P. Ziegler−Natta-like Olefin Oligomerization by Alkylzirconocene Cations in an Electrospray Ionization Tandem Mass Spectrometer. *J. Am. Chem. Soc.* **1998**, *120*, 7125−7126.

(17) Resconi, L.; Cavallo, L.; Fait, A.; Piemontesi, F. Selectivity in Propene Polymerization with Metallocene Catalysts. *Chem. Rev.* **2000**, *100*, 1253−1346.

(18) Lieber, S.; Prosenc, M.-H.; Brintzinger, H.-H. Zirconocene Allyl Complexes: Dynamics in Solution, Reaction with Aluminum Alkyls, B(C6F5)3-Induced Propene Insertion, and Density-Functional Calculations on Possible Formation and Reaction Pathways. *Organometallics* **2000**, *19*, 377−387.

(19) Panchenko, V. N.; Babushkin, D. E.; Bercaw, J. E.; Brintzinger, H. H. Catalyst Speciation during ansa-Zirconocene-Catalyzed Polymerization of 1-Hexene Studied by UV-vis Spectroscopy-Formation and Partial Re-Activation of Zr-Allyl Intermediates. *Polymers* **2019**, *11*, 936.

(20) Al-Humydi, A.; Garrison, J. C.; Mohammed, M.; Youngs, W. J.; Collins, S. Propene Polymerization Using Ansa-Metallocenium Ions: Catalyst Deactivation Processes during Monomer Consumption and Molecular Structures of the Products Formed. *Polyhedron* **2005**, *24*, 1234−1249.

(21) Moscato, B. M.; Zhu, B.; Landis, C. R. Mechanistic Investigations into the Behavior of a Labeled Zirconocene Polymerization Catalyst. *Organometallics* **2012**, *31*, 2097−2107.

(22) Panchenko, V. N.; Babushkin, D. E.; Brintzinger, H. H. Zirconium-Allyl Complexes as Resting States in Zirconocene-Catalyzedα-Olefin Polymerization. *Macromol. Rapid Commun.* **2015**, *36*, 249−253.

(23) Bryliakov, K. P.; Talsi, E. P.; Semikolenova, N. V.; Zakharov, V. A.; Brand, J.; Alonso-Moreno, C.; Bochmann, M. Formation and structures of cationic zirconium complexes in ternary systems (X=Cl, Me). *J. Organomet. Chem.* **2007**, *692*, 859−868.

(24) Baldwin, S. M.; Bercaw, J. E.; Henling, L. M.; Day, M. W.; Brintzinger, H. H. Cationic Alkylaluminum-Complexed Zirconocene Hydrides: NMR-Spectroscopic Identification, Crystallographic Structure Determination, and Interconversion with Other Zirconocene Cations. *J. Am. Chem. Soc.* **2011**, *133*, 1805−1813.

(25) Ewen, J. A.; Elder, M. J. Syntheses and Models for Stereospecific Metallocenes. *Makromol. Chem., Macromol. Symp.* **1993**, *66*, 179−190.

(26) Chien, J. C. W.; Tsai, W. M.; Rausch, M. D. Isospecific Polymerization of Propylene Catalyzed by Rac-Ethylenebis(Indenyl)-Methylzirconium Cation. *J. Am. Chem. Soc.* **1991**, *113*, 8570−8571.

(27) Song, F.; Cannon, R. D.; Bochmann, M. Zirconocene-Catalyzed Propene Polymerization: A Quenched-Flow Kinetic Study. *J. Am. Chem. Soc.* **2003**, *125*, 7641−7653.

(28) Fisch, A. G.; dos Santos, J. H. Z.; Cardozo, N. S. M.; Secchi, A. R. Mass Transfer in Olefin Polymerization: Estimative of Macro- and Microscale Diffusion Coefficients through the Swollen Polymer. *Chem. Eng. Sci.* **2008**, *63*, 3727−3739.

(29) Song, F.; Cannon, R. D.; Bochmann, M. The kinetics of propene and hexene polymerisation with [(SBI)ZrR]+X−: evidence for

monomer-dependent early or late transition states. *Chem. Commun.* **2004**, *4*, 542−543.
(30) Kissin, Y. V. Oligomerization Reactions of 1-Hexene with Metallocene Catalysts: Detailed Data on Reaction Chemistry and Kinetics. *Mol. Catal.* **2019**, *463*, 87−93.
(31) Camara, J. M.; Petros, R. A.; Norton, J. R. Zirconium-Catalyzed Carboalumination of α-Olefins and Chain Growth of Aluminum Alkyls: Kinetics and Mechanism. *J. Am. Chem. Soc.* **2011**, *133*, 5263−5273.
(32) Trefz, T. K.; Henderson, M. A.; Wang, M. Y.; Collins, S.; McIndoe, J. S. Mass Spectrometric Characterization of Methylaluminoxane. *Organometallics* **2013**, *32*, 3149−3152.
(33) Trefz, T. K.; Henderson, M. A.; Linnolahti, M.; Collins, S.; McIndoe, J. S. Mass Spectrometric Characterization of Methylaluminoxane-Activated Metallocene Complexes. *Chem.—Eur. J.* **2015**, *21*, 2980−2991.
(34) Zijlstra, H. S.; Linnolahti, M.; Collins, S.; McIndoe, J. S. Additive and Aging Effects on Methylalumoxane Oligomers. *Organometallics* **2017**, *36*, 1803−1809.
(35) Zijlstra, H. S.; Collins, S.; McIndoe, J. S. Oxidation of Methylalumoxane Oligomers. *Chem.—Eur. J.* **2018**, *24*, 5506−5512.
(36) Endres, E.; Zijlstra, H. S.; Collins, S.; McIndoe, J. S.; Linnolahti, M. Oxidation of Methylalumoxane Oligomers: A Theoretical Study Guided by Mass Spectrometry. *Organometallics* **2018**, *37*, 3936−3942.
(37) Zijlstra, H. S.; Harder, S. Methylalumoxane—History, Production, Properties, and Applications. *Eur. J. Inorg. Chem.* **2015**, *2015*, 19−43.
(38) Velthoen, M. E. Z.; Muñoz-Murillo, A.; Bouhmadi, A.; Cecius, M.; Diefenbach, S.; Weckhuysen, B. M. The Multifaceted Role of Methylaluminoxane in Metallocene-Based Olefin Polymerization Catalysis. *Macromolecules* **2018**, *51*, 343−355.
(39) Kilpatrick, A. F. R.; Rees, N. H.; Sripothongnak, S.; Buffet, J.-C.; O'Hare, D. Slurry-Phase Ethylene Polymerization Using Pentafluorophenyl- and Pentafluorophenoxy-Modified Solid Polymethylaluminoxanes. *Organometallics* **2018**, *37*, 156−164.
(40) Collins, S.; Linnolahti, M.; Zamora, M. G.; Zijlstra, H. S.; Rodríguez Hernández, M. T.; Perez-Camacho, O. Activation of Cp2ZrX2 (X = Me, Cl) by Methylaluminoxane As Studied by Electrospray Ionization Mass Spectrometry: Relationship to Polymerization Catalysis. *Macromolecules* **2017**, *50*, 8871−8884.
(41) Lancaster, S. J.; Robinson, O. B.; Bochmann, M.; Coles, S. J.; Hursthouse, M. B. Synthesis and Reactivity of New Mono-(Cyclopentadienyl)Zirconium and -Hafnium Alkyl Complexes. Crystal and Molecular Structure of [{C5H3(SiMe3)2}HfMe2(.Eta.6-Toluene)][BMe(C6F5)3]. *Organometallics* **1995**, *14*, 2456−2462.
(42) Vikse, K. L.; Woods, M. P.; McIndoe, J. S. Pressurized Sample Infusion for the Continuous Analysis of Air- And Moisture-Sensitive Reactions Using Electrospray Ionization Mass Spectrometry. *Organometallics* **2010**, *29*, 6615−6618.
(43) Zaccaria, F.; Sian, L.; Zuccaccia, C.; Macchioni, A. Ion Pairing in Transition Metal Catalyzed Olefin Polymerization. *Adv. Organomet. Chem.* **2020**, *73*, 1−78.
(44) Yang, S. H.; Huh, J.; Jo, W. H. Effect of Solvent Polarity on the Initiation and the Propagation of Ethylene Polymerization with Constrained Geometry Catalyst/MAO Catalytic System: A Density Functional Study with the Conductor-like Screening Model. *Macromolecules* **2005**, *38*, 1402−1409.
(45) Forlini, F.; Fan, Z.-Q.; Tritto, I.; Locatelli, P.; Sacchi, M. C. Metallocene-Catalyzed Propene/1-Hexene Copolymerization: Influence of Amount and Bulkiness of Cocatalyst and of Solvent Polarity. *Macromol. Chem. Phys.* **1997**, *198*, 2397−2408.
(46) Talsi, E. P.; Eilertsen, J. L.; Ystenes, M.; Rytter, E. 1H-NMR spectroscopic study of cationic intermediates in solvent and oil constituents of the catalytic systems Cp2ZrMe2/[CPh3][B(C6F5)4] and Cp2ZrMe2/AlMe3/[CPh3][B(C6F5)4] in benzene. *J. Organomet. Chem.* **2003**, *677*, 10−14.
(47) Bochmann, M.; Lancaster, S. J. Monomer-Dimer Equilibria in Homo- and Heterodinuclear Cationic Alkylzirconium Complexes and Their Role in Polymerization Catalysis. *Angew. Chem., Int. Ed. Engl.* **1994**, *33*, 1634−1637.
(48) Bochmann, M.; Sarsfield, M. J. Reaction of AlR3with [CPh3][B(C6F5)4]: Facile Degradation of [B(C6F5)4]-by Transient "[AlR2]+". *Organometallics* **1998**, *17*, 5908−5912.
(49) Beck, S.; Prosenc, M.-H.; Brintzinger, H.-H.; Goretzki, R.; Herfert, N.; Fink, G. Binuclear zirconocene cations with μ-CH3-bridges in homogeneous Ziegler-Natta catalyst systems. *J. Mol. Catal. Chem.* **1996**, *111*, 67−79.
(50) Wu, F.; Dash, A. K.; Jordan, R. F. Structures and Reactivity of Zr(IV) Chlorobenzene Complexes. *J. Am. Chem. Soc.* **2004**, *126*, 15360−15361.
(51) Černý, Z.; Fusek, J.; Kříž, O.; Heřmánek, S.; Šolc, M.; Čásenský, B. 27Al NMR Study of the Trimethylaluminum Monomer-Dimer Equilibrium. *J. Organomet. Chem.* **1990**, *386*, 157−165.
(52) Babu, G. N.; Newmark, R. A.; Chien, J. C. W. Microstructure of Poly(1-Hexene) Produced by Ansa-Zirconocenium Catalysis. *Macromolecules* **1994**, *27*, 3383−3388.
(53) Brintzinger, H. H.; Fischer, D.; Mülhaupt, R.; Rieger, B.; Waymouth, R. M. Stereospecific Olefin Polymerization with Chiral Metallocene Catalysts. *Angew. Chem., Int. Ed. Engl.* **1995**, *34*, 1143−1170.
(54) Lanzinger, D.; Höhlein, I. M.; Weiß, S. B.; Rieger, B. Catalytic C-F Activation via Cationic Group IV Metallocenes. *J. Organomet. Chem.* **2015**, *778*, 21−28.
(55) Joshi, A.; Donnecke, S.; Granot, O.; Shin, D.; Collins, S.; Paci, I.; Scott McIndoe, J. Reactive Metallocene Cations as Sensitive Indicators of Gas-Phase Oxygen and Water. *Dalton Trans.* **2020**, *49*, 7028.
(56) Vikse, K. L.; Ahmadi, Z.; Luo, J.; van der Wal, N.; Daze, K.; Taylor, N.; McIndoe, J. S. Pressurized Sample Infusion: An Easily Calibrated, Low Volume Pumping System for ESI-MS Analysis of Reactions. *Int. J. Mass Spectrom.* **2012**, *323*−*324*, 8−13.
(57) Hesketh, A. V.; Nowicki, S.; Baxter, K.; Stoddard, R. L.; McIndoe, J. S. Simplified Real-Time Mass Spectrometric Analysis of Reactions. *Organometallics* **2015**, *34*, 3816−3819.
(58) Bryliakov, K. P.; Talsi, E. P.; Voskoboynikov, A. Z.; Lancaster, S. J.; Bochmann, M. Formation and Structures of Hafnocene Complexes in MAO- and AlBui3/CPh3[B(C6F5)4]-Activated Systems. *Organometallics* **2008**, *27*, 6333−6342.
(59) Pike, S. D.; Crimmin, M. R.; Chaplin, A. B. Organometallic Chemistry Using Partially Fluorinated Benzenes. *Chem. Commun.* **2017**, *53*, 3615−3633.
(60) Al-Humydi, A.; Youngs, W. J.; Collins, S. Propene Polymerization Usingansa-Metallocenium Ions: Excess Activator Effects on Polymerization Activity and Polymer Microstructure. *Organometallics* **2005**, *24*, 1784.
(61) Götz, C.; Rau, A.; Luft, G. Ternary metallocene catalyst systems based on metallocene dichlorides and AlBu3i/[PhNMe2H][B(C6F5)-4]. *J. Mol. Catal. Chem.* **2002**, *184*, 95−110.
(62) Downs, A. J.; Greene, T. M.; Collin, S. E.; Whitehurst, L. A.; Brain, P. T.; Morrison, C. A.; Pulham, C. R.; Smart, B. A.; Rankin, D. W. H.; Keys, A.; Barron, A. R. Dimethylalane, [Me2AlH]n, in the Vapor Phase and in Hydrocarbon Solution: Gas-Phase Electron Diffraction, Spectroscopic, Colligative, and ab Initio Studies. *Organometallics* **2000**, *19*, 527−538.
(63) Pankratyev, E. Y.; Khursan, S. L.; Tyumkina, T. V.; Khalilov, L. M. A quantum chemical study of self-association of HAlBu 2 i and ClAlBu 2 i. *J. Struct. Chem.* **2011**, *52*, 27−34.
(64) Busico, V.; Cipullo, R.; Romanelli, V.; Ronca, S.; Togrou, M. Reactivity of Secondary Metal−Alkyls in Catalytic Propene Polymerization: How Dormant Are "Dormant Chains"? *J. Am. Chem. Soc.* **2005**, *127*, 1608−1609.

https://dx.doi.org/10.1021/acscatal.0c01607
ACS Catal. 2020, 10, 7195−7206